JOURNAL OF GUIDANCE, CONTROL, AND DYNAMICS
Vol. 27, No. 1, January-February 2004, pp. 118 - 126.

Integrated Guidance and Control of Moving Mass Actuated Kinetic Warheads

P. K. Menon[*], G. D. Sweriduk[†]
Optimal Synthesis Inc., Los Altos, CA
E. J. Ohlmeyer[‡], D. S. Malyevac[§]
Naval Surface Warfare Center, Dahlgren, VA

Abstract

Modeling, simulation, and integrated guidance-control of a kinetic warhead utilizing moving-mass actuators are discussed. Moving masses can be used in any speed range both in the atmosphere as well as outside it, as long as there is a force, either aerodynamic or propulsive, acting on the vehicle. The moving-mass actuation technique offers significant advantages over conventional aerodynamic control surfaces and reaction control systems, since the actuators are contained entirely within the airframe geometric envelope and produce no plumes. The present research develops a nine degree-of-freedom simulation model of a kinetic warhead with three moving-mass actuators. This simulation model is used for actuator sizing and in the development of flight control systems. A software package for performing numerical feedback linearization is employed for the design of nonlinear flight control systems. Interception of non-maneuvering and weaving targets in both endo-atmospheric and exo-atmospheric conditions is demonstrated.

1. Introduction

Some of the earliest flight vehicles were controlled by moving the body of the pilot[1,2] to effect a change in the center of mass of the vehicle. The change in vehicle center of mass alters the relative location of the center of mass with respect to the external forces, thereby effecting a change in the vehicle's motion. Advances in

[*] Chief Scientist, 868 San Antonio Road, Palo Alto, CA 94303-4622. Associate Fellow AIAA
[†] Research Scientist, 868 San Antonio Road, Palo Alto, CA 94303-4622. Senior Member AIAA
[‡] Group Leader, Missile Systems Division, Code G23, 17320 Dahlgren Road, Dahlgren, VA 22448, Associate Fellow AIAA
[§] Senior Mechanical Engineer, Code G23, 17320 Dahlgren Road, Dahlgren, VA 22448, Member AIAA

aerodynamics subsequently made the moving-mass approach to flight control obsolete in all but a few, specialized applications. A present-day use of moving-mass control can be found on hang-gliders, wherein the pilot changes the relative location of his/her body with respect to the lifting plane to effect changes in flight path. Although mass movement control is no longer used on commercial flight vehicles, it continues to be important in applications such as the control of reentry vehicles at extreme Mach numbers, where the aerodynamic heating and drag penalties can make it impractical to deploy flight control surfaces[3,4].

Recently, mass movement has been proposed as a control methodology for a kinetic warhead (KW) in atmospheric and exo-atmospheric engagements[5]. As illustrated in Figure 1, the moving-mass control system changes the vehicle center of mass relative to the external forces to generate the desired control moments. For instance, if the thrust is

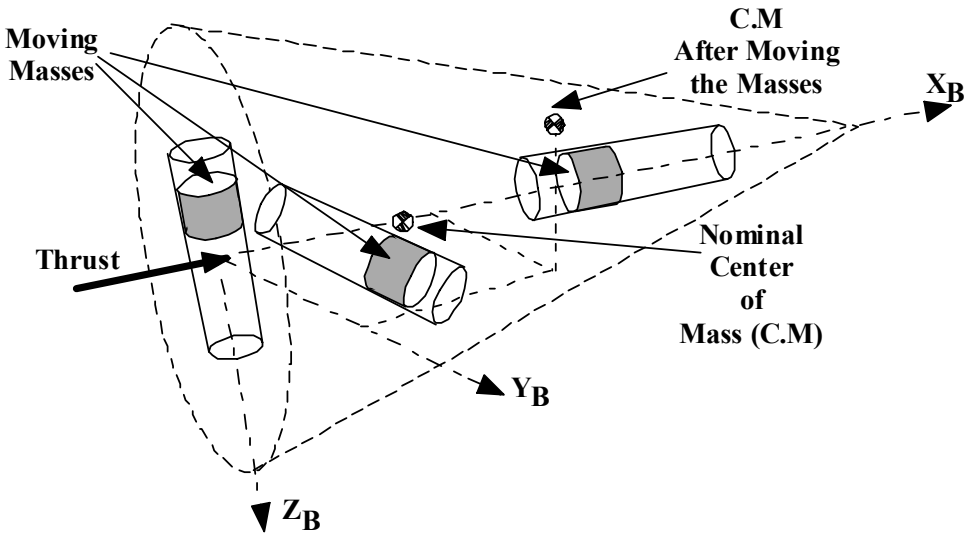

aligned with the vehicle longitudinal body axis containing the nominal center of mass as shown in

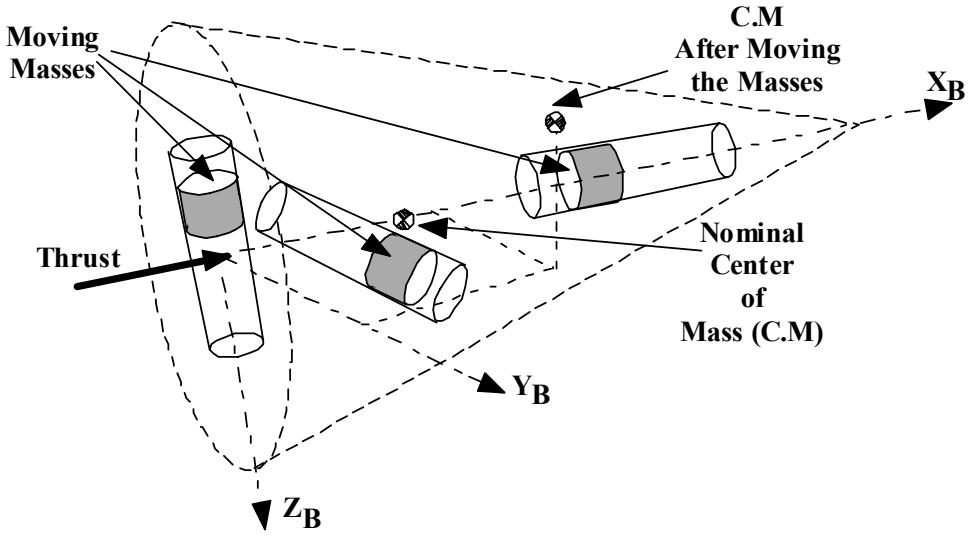

Figure 1, moving the center of mass off the body centerline will result in thrust moments about the pitch - yaw axes. Additionally, roll moments will be generated if the thrust or drag has an angular misalignment with respect to the longitudinal axis, or if the vehicle is subject to an aerodynamic lift force. The moving-mass control concept works equally well in space when the KW is thrusting, or in the atmosphere, when the vehicle experiences aerodynamic forces. Thus, this actuation technology can be employed in kinetic warheads that have both atmospheric and exo- atmospheric interception capabilities.

While the design of flight control systems using moving-mass actuation appears to be conceptually straightforward, difficulties arise due to the highly coupled and nonlinear nature of the system dynamics. This is partly due to the fact that in addition to causing changes in the vehicle center of mass, the moving-mass control system will exert inertial forces on the airframe. Moreover, the moving masses will change the instantaneous moments and products of inertia of the flight vehicle, which will then contribute to changes in the dynamic response. The KW control system design must deliver the desired interception accuracy while accommodating these dynamic effects.

Previous research has demonstrated that integrated design of guidance-autopilot systems can deliver fast-responding flight control systems by exploiting synergy between the vehicle attitude dynamics and the translational dynamics. Recently, integrated design techniques have been investigated in the context of guidance-autopilot-fuze-warhead

system design for ship-defense missiles[6,7]. Three distinct methodologies were developed and results were obtained for the state dependent Riccati equation technique[8,9,10] and the feedback linearization approach[11–15]. The research discussed in Reference 6 was primarily motivated by the advancements in missile sensor and warhead technologies. A recent research effort[16] focused on the development of integrated guidance-autopilot systems for a fixed-aim warhead missile. Integrated design techniques developed under these research efforts form the starting point for the present development of moving-mass guidance-autopilot system for a KW.

The objective of the present research is to establish the feasibility of designing moving-mass actuated flight control systems for kinetic warheads that will meet the accuracy requirements in both exo-atmospheric and atmospheric target interception scenarios. This feasibility demonstration is achieved through a nonlinear engagement simulation of a moving-mass controlled KW intercepting a tactical ballistic missile in various stages of flight.

An integrated guidance-autopilot system based on the feedback linearization technique was synthesized using recently developed, computer-aided, nonlinear control system design software[17]. This software was developed under a previous research effort[18,19]. A unique feature of this software package is that it permits the direct synthesis of nonlinear control systems from computer simulation models of dynamic systems.

The following sections will discuss vehicle modeling, guidance-autopilot system design and evaluation in example engagement scenarios. Detailed modeling of a KW with moving-mass actuators will be given in Section 2. Flight control system designs and engagement simulation results will be presented Section 3. Conclusions from the present research will be given in Section 4.

2. Moving Mass Actuated Kinetic Warhead Model

This section will present the formulation of a 9 degree-of-freedom model of the kinetic warhead with moving-mass actuators. The equations of motion were coded in FORTRAN and then used in conjunction with Simulink[20] to produce a simulation of the kinetic warhead.

2.1 Kinetic Warhead Model

In the present study, the kinetic warhead consists of a cone-shaped body with three actuator masses that can move parallel to the three orthogonal axes of the vehicle. A free-body diagram of the kinetic warhead is shown in Figure 2.

In addition to the acceleration due to gravity, the kinetic warhead will experience aerodynamic forces in atmospheric flight. In exo-atmospheric flight, thrust is the dominant external force that acts on the vehicle.

2.1.1 Nomenclature

The following notation is used in deriving the equations of motion (see Figure 2):

- m_B is the mass of the kinetic warhead body B.
- m_x, m_y, m_z are the actuator masses moving parallel to the body x, y, and z axes, respectively.
- m_T is the total mass of the kinetic warhead and the actuator masses
- $V_O = [u \;\; v \;\; w]^T$ is the inertial velocity vector of the center of mass of the vehicle body B.
- $\omega_B = [p \;\; q \;\; r]^T$ is the inertial angular velocity vector of the body B.
- $p_x = \begin{bmatrix} \delta_x \\ y_{offset} \\ 0 \end{bmatrix}, \; p_y = \begin{bmatrix} -x_{offset} \\ \delta_y \\ 0 \end{bmatrix}, \; p_z = \begin{bmatrix} -x_{offset} \\ 0 \\ \delta_z \end{bmatrix}$

  are the position vectors of the actuator masses in the body frame centered at the vehicle center of mass. The mass offsets x_{offset}, y_{offset} are assumed to be specified. The variables δ_x, δ_y, and δ_z are the displacements of the three masses.
- $\dot{p}_x = \begin{bmatrix} \dot{\delta}_x \\ 0 \\ 0 \end{bmatrix}, \; \dot{p}_y = \begin{bmatrix} 0 \\ \dot{\delta}_y \\ 0 \end{bmatrix}, \; \dot{p}_z = \begin{bmatrix} 0 \\ 0 \\ \dot{\delta}_z \end{bmatrix}$ are the relative velocities of the actuator masses with respect to the body B.
- $b_1^T = \begin{bmatrix} 1 \\ 0 \\ 0 \end{bmatrix}, \; b_2^T = \begin{bmatrix} 0 \\ 1 \\ 0 \end{bmatrix}, \; b_3^T = \begin{bmatrix} 0 \\ 0 \\ 1 \end{bmatrix}$ are orthonormal basis vectors.

- u_x, u_y, u_z are the control forces acting on the x, y, and z axis actuator masses, respectively.
- $I_{B/O}$ is the 3×3 inertia tensor of the body B about its center of mass.
- r_{CP} is the position vector of the aerodynamic center of pressure from the center of mass of body B. The center of pressure is the theoretical point at which the aerodynamic forces act, and about which there is no aerodynamic moment.
- r_T is the position vector of the point of application of the external thrust vector T from the center of mass of body B.
- F is the vector of aerodynamic forces at the center of pressure in the body frame.
- M is the vector of aerodynamic moments about the center of pressure in the body frame.
- T is the thrust vector in the body frame.
- $a_g = \begin{bmatrix} 0 \\ 0 \\ g \end{bmatrix}$ is the gravity vector in the inertial frame. The acceleration due to gravity is given by: $g = 32.174\left(\frac{R_E}{R_E + h}\right)^2$ where h is altitude. $R_E = 2.0925 \times 10^7$ ft is the mean radius of the earth.
- C_{NB} is the transformation matrix from the body frame to the inertial frame.

The equations of motion of the kinetic warhead are derived using Kane's method[21]. The mathematical model consists of the dynamical and kinematical equations given in the two following subsections.

2.1.2 Dynamical Equations

The kinetic warhead translational dynamics are given by Equation (1).

$$\begin{aligned} & m_T \dot{V}_O - \left(m_x p_x + m_y p_y + m_z p_z\right) \times \dot{\omega}_B + m_x \ddot{p}_x + m_y \ddot{p}_y + m_z \ddot{p}_z \\ & = -\omega_B \times \left\{ m_T V_O + m_x \left(\omega_B \times p_x + 2\dot{p}_x\right) + m_y \left(\omega_B \times p_y + 2\dot{p}_y\right) + m_z \left(\omega_B \times p_z + 2\dot{p}_z\right) \right\} \\ & \quad + F + m_T C_{NB}^T a_g + T \end{aligned} \tag{1}$$

The vehicle rotational dynamics are given by Equation (2).

$$
\begin{aligned}
&\left(m_x p_x + m_y p_y + m_z p_z\right)\times \dot{V}_O + I_{B/O}\dot{\omega}_B \\
&- m_x p_x \times \left(p_x \times \dot{\omega}_B\right) - m_y p_y \times \left(p_y \times \dot{\omega}_B\right) - m_z p_z \times \left(p_z \times \dot{\omega}_B\right) \\
&+ m_x p_x \times \ddot{p}_x + m_y p_y \times \ddot{p}_y + m_z p_z \times \ddot{p}_z \\
&= -\{\ \omega_B \times I_{B/O}\omega_B + m_x p_x \times \omega_B \times \left(V_O + \omega_B \times p_x + 2\dot{p}_x\right) \\
&+ m_y p_y \times \omega_B \times \left(V_O + \omega_B \times p_y + 2\dot{p}_y\right) + m_z p_z \times \omega_B \times \left(V_O + \omega_B \times p_z + 2\dot{p}_z\right)\ \} \\
&+ M + \left(r_{CP} \times F\right) + \left(r_{TH} \times T\right) + \left(m_x p_x + m_y p_y + m_z p_z\right)\times C_{NB}^T a_g
\end{aligned}
\tag{2}
$$

The motions of the actuator masses are described by Equations (3) – (5).

$$
\begin{aligned}
&m_x b_1^T\left(\ \dot{V}_O - p_x \times \dot{\omega}_B\ \right) + m_x \ddot{\delta}_x = \\
&- m_x b_1^T\left[\omega_B \times \left(V_O + \omega_B \times p_x + 2\dot{p}_x\right) - C_{NB}^T a_g\right] + u_x
\end{aligned}
\tag{3}
$$

$$
\begin{aligned}
&m_y b_2^T\left(\ \dot{V}_O - p_y \times \dot{\omega}_B\ \right) + m_y \ddot{\delta}_y = \\
&- m_y b_2^T\left[\omega_B \times \left(V_O + \omega_B \times p_y + 2\dot{p}_y\right) - C_{NB}^T a_g\right] + u_y
\end{aligned}
\tag{4}
$$

$$
\begin{aligned}
&m_z b_3^T\left(\ \dot{V}_O - p_z \times \dot{\omega}_B\ \right) + m_z \ddot{\delta}_z = \\
&- m_z b_3^T\left[\omega_B \times \left(V_O + \omega_B \times p_z + 2\dot{p}_z\right) - C_{NB}^T a_g\right] + u_z
\end{aligned}
\tag{5}
$$

At each value of the state vector, the nine dynamical equations in (1) – (5) can be solved as a system of linear equations to obtain the state rates of the system dynamics:

$$
A(x)\begin{bmatrix} \dot{V}_O \\ \dot{\omega}_B \\ \ddot{\delta}_x \\ \ddot{\delta}_y \\ \ddot{\delta}_z \end{bmatrix} = f(x,u) \tag{6}
$$

where x is the state vector and $A(x)$ is a 9×9 matrix, and $f(x,u)$ is a vector of the sums of forces and moments. State rates from (6) can be used in conjunction with numerical integration algorithms to generate temporal histories of the state variables. The dynamical equations have to be augmented with the kinematical equations given in the next section to complete the description of the KW dynamics.

2.1.3 Kinematical Equations

The inertial-frame position of the mass center of the vehicle body B is given by Equation (7).

$$\begin{pmatrix} \dot{x} \\ \dot{y} \\ \dot{z} \end{pmatrix} = \begin{bmatrix} 1-2(q_2^2+q_3^2) & 2(q_1q_2-q_3q_4) & 2(q_1q_3+q_2q_4) \\ 2(q_1q_2+q_3q_4) & 1-2(q_1^2+q_3^2) & 2(q_2q_3-q_1q_4) \\ 2(q_1q_3-q_2q_4) & 2(q_2q_3+q_1q_4) & 1-2(q_1^2+q_2^2) \end{bmatrix} (V_O) = C_{NB}V_O \quad (7)$$

where $q_1 - q_4$ are the Euler parameters or quaternions.

The temporal evolution of the quaternions is governed by the differential equation (8):

$$\begin{pmatrix} \dot{q}_1 \\ \dot{q}_2 \\ \dot{q}_3 \\ \dot{q}_4 \end{pmatrix} = 0.5 \begin{bmatrix} q_4 & -q_3 & q_2 \\ q_3 & q_4 & -q_1 \\ -q_2 & q_1 & q_4 \\ -q_1 & -q_2 & -q_3 \end{bmatrix} (\omega_B) \quad (8)$$

2.1.4 Kinetic Warhead Properties

The values of the various physical properties of the kinetic warhead are as follows. These were obtained from Reference 5:

m_B = 55 lbm or 1.7095 slugs

$m_x = m_y = m_z$ = 5 lbm. or 0.1554 slugs

$I_{B/O} = \begin{bmatrix} 0.12821 & 0 & 0 \\ 0 & 0.6 & 0 \\ 0 & 0 & 0.6 \end{bmatrix}$ slug-ft^2, where the I_{11} term was computed assuming a solid right circular cone with a base diameter d = 1 ft, and I_{22} and I_{33} are from Reference 5.

The thrust vector T used for exo-atmospheric engagements was [500 0 0]^T lbf.

2.1.5 Aerodynamic Model

The normal and axial forces due to aerodynamics are computed using the expressions:

$$\begin{aligned} &F_N = \overline{Q} S_{ref} C_N, \quad F_x = -\overline{Q} S_{ref} C_A, \\ &\overline{Q} = \tfrac{1}{2}\rho V^2, \quad S_{ref} = \pi d^2/4 = (\pi/4) \end{aligned} \quad (9)$$

where the coefficients C_N and C_A are interpolated from tabular data, and V is the total velocity, the magnitude of the inertial velocity vector whose body-axis components are u,

v, and *w*. The aerodynamic coefficients are specified as functions of Mach number and the total angle of attack α_T

$$\alpha_T = cos^{-1}\left(\frac{u}{V}\right) \tag{10}$$

The normal force F_N is resolved into the body-axis *y* and *z* components as:

$$F_y = \frac{v}{\sqrt{v^2 + w^2}} F_N, \quad F_z = \frac{w}{\sqrt{v^2 + w^2}} F_N \tag{11}$$

Aerodynamic moment coefficients were not available at the time of this study. Hence, the aerodynamic moments are computed using the lift and drag forces acting at the aerodynamic center, with the static margin as the lever arm. The static margin was set to 0.01 ft for all the simulations given in this paper. The location of the aerodynamic center is assumed to be independent of Mach number and total angle of attack. Aerodynamic damping and unsteady aerodynamic effects are neglected.

Atmospheric density and the speed of sound were computed using the 1976 U.S. standard atmosphere model. In the present study, the atmospheric model is defined for altitudes up to 435 miles, although aerodynamic effects are expected to be insignificant above about 37 miles.

2.1.6 Moving-Mass Positioning Actuator Model

The displacements of the actuator masses are limited (0.5 ft.) since the mass cannot travel beyond the geometric envelope of the vehicle. These constraints are enforced by adding constraint forces to the equations of motion so as to bring the velocity of the moving masses to zero when the displacement approaches its limit and to counter the actuator force as long as it pushes the mass against the stop. Moreover, limits were also imposed on the control forces applied by the servos (200 lbf.).

The longitudinal moving mass was not used for control in the present study and was held in place by a proportional plus derivative servo. The servo gains are chosen to yield an undamped natural frequency of 50 Hz, with 0.71 damping ratio. In response to a commanded displacement of δ_{ic} the actuator servo will apply a force

$$F_i = -k_p\left(\delta_i - \delta_{i_c}\right) - k_d\dot{\delta}_i \tag{12}$$

on the moving mass. The proportional gain k_p (lbf/ft) and the derivative gain k_d (lbf/ft/s) corresponding to actuator natural frequency and damping can be computed as 15340 and 70, respectively. Note that these gains correspond to a moving mass of 0.1554 slugs (5 lb).

2.1.7 Line-of-Sight Angles and Rates

In addition to the equations of motion, the guidance law computations require the line-of-sight angles and rates. The definition of line-of-sight (LOS) angles λ_y, λ_z are illustrated in

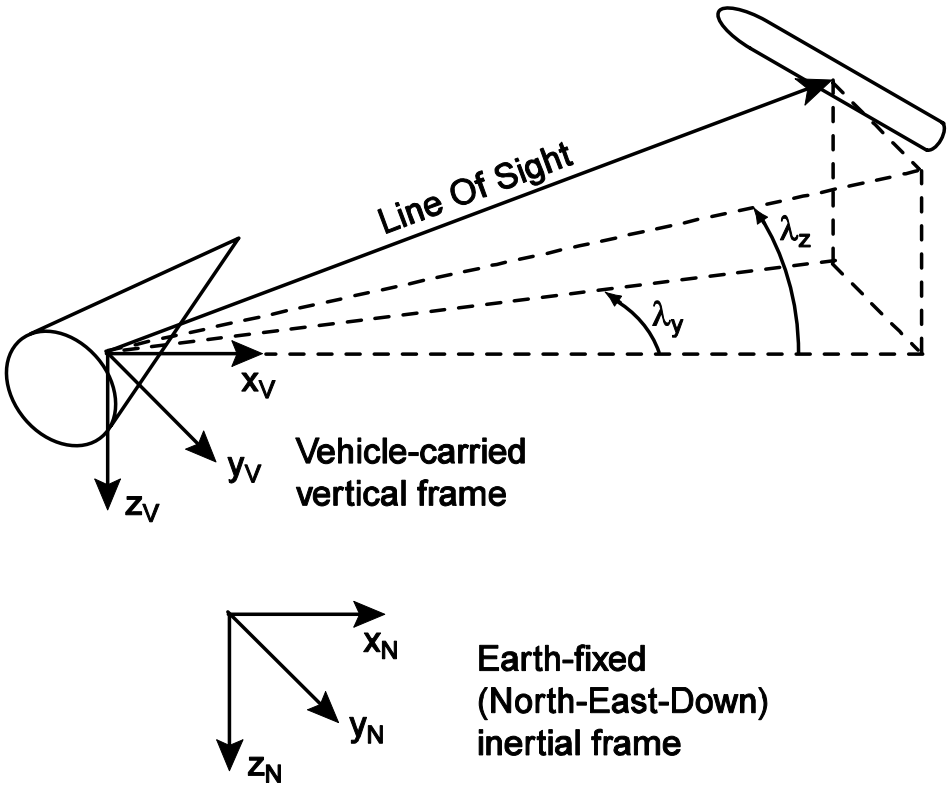

Figure 3. The missile relative-target position vector, or the line-of-sight, in the inertial frame is

$$\vec{r} = \vec{r}_t - \vec{r}_{kw} \tag{13}$$

where $\vec{r}_t = \begin{bmatrix} x_t & y_t & z_t \end{bmatrix}^T$ and $\vec{r}_{kw} = \begin{bmatrix} x_{kw} & y_{kw} & z_{kw} \end{bmatrix}^T$ are the inertial position vectors of the target and the kinetic warhead, respectively. Let $\vec{r} = \begin{bmatrix} r_x & r_y & r_z \end{bmatrix}^T$. The line-of-sight angles can then be defined as:

$$\lambda_y = tan^{-1}\left(\frac{r_y}{r_x}\right), \lambda_z = tan^{-1}\left(\frac{r_z}{r_x}\right) \tag{14}$$

The difference between the inertial velocity vectors, expressed in the Earth-fixed inertial frame, is the relative velocity, represented by $\dot{\vec{r}} = \begin{bmatrix}\dot{r}_x & \dot{r}_y & \dot{r}_z\end{bmatrix}^T = V_t - C_{NB}V_O$. The line-of-sight angular rates are obtained by taking the time derivatives of the LOS angles in (14):

$$\dot{\lambda}_y = \frac{\dot{r}_y - \dot{r}_x \tan\lambda_y}{r_x \sec^2\lambda_y} = \frac{r_x\dot{r}_y - \dot{r}_x r_y}{r^2}, \quad \dot{\lambda}_z = \frac{\dot{r}_z - \dot{r}_x \tan\lambda_z}{r_x \sec^2\lambda_z} = \frac{r_x\dot{r}_z - \dot{r}_x r_z}{r^2} \tag{15}$$

where $r = \left(r_x^2 + r_y^2 + r_z^2\right)^{1/2}$.

The expressions for angular acceleration of the LOS angle required in the integrated flight control system designs can be computed from the following geometric relationships:

$$\ddot{\lambda}_y = \frac{r\left(r_x\ddot{r}_y - \ddot{r}_x r_y\right) - 2\dot{r}\left(r_x\dot{r}_y - \dot{r}_x r_y\right)}{r^3}, \quad \ddot{\lambda}_z = \frac{r\left(r_x\ddot{r}_z - \ddot{r}_x r_z\right) - 2\dot{r}\left(r_x\dot{r}_z - \dot{r}_x r_z\right)}{r^3} \tag{16}$$

where the relative inertial acceleration is $\ddot{\vec{r}} = \begin{bmatrix}\ddot{r}_x & \ddot{r}_y & \ddot{r}_z\end{bmatrix}^T = a_t - a_{kw}$. The inertial acceleration of the kinetic warhead is $a_{kw} = C_{NB}\left(\dot{V}_O + \omega_B \times V_O\right)$, and the acceleration of the target a_t is generally unknown, and needs to be estimated by the flight control system.

2.2 Target Model

A non-maneuvering target and a weaving target model are considered in the present research. The accelerations of the target in the inertial frame are:

$$\ddot{x} = 0, \quad \ddot{y} = 0, \quad \ddot{z} = g \quad OR \quad \ddot{z} = A\,\omega^2 \sin\omega t \tag{17}$$

As can be garnered from the Equation (17), the nonmaneuvering target is assumed to be falling under the action of gravity. The weaving target model is assumed to be capable of 3 g normal acceleration with a frequency of 0.5 Hz.

3. Guidance and Control System Design

The dynamic model of the kinetic warhead described in Section 2 is used to develop control and guidance laws. This section will present the design of guidance and

control laws for atmospheric and exo-atmospheric interception scenarios. The feedback linearization technique[11–15] is used to design nonlinear control laws using the complete model of the kinetic warhead. The feedback linearization methodology transforms a given nonlinear dynamic model into a linear, time-invariant (Brunovsky canonical) form using a state-dependent map. Any linear control methodology can then be used to design the control system. Inverse transformation of the control law to the original coordinates then yields the nonlinear control law. Appendix A briefly outlines the feedback linearization process for the integrated guidance-control problem. The results given in this paper were obtained using the pole placement design technique in conjunction with the feedback linearization approach.

A software package for feedback linearization developed under a previous research effort[19] is used in the design process. Given the simulation model of a dynamic system in standard form[17], the hierarchy of the states in the system, and their relationships to the control variables, the software package automatically generates a feedback linearizing map, and the transformed system dynamics. Control law design using the transformed dynamics, together with the inverse of the feedback linearizing map, are then used to compute the nonlinear control law.

The following section will discuss the integrated flight control system design. The integrated design methodology simultaneously addresses the guidance and autopilot design problems. An advantage of the integrated design methodology is that it eliminates the iterations between guidance and autopilot design processes required for satisfying the flight control system performance objectives. Detailed discussions on the benefits of the integrated design methodology are given in References 7, 16, 22, and 23.

3.1 Integrated Design Based on Line-of-Sight Rate Regulation

This integrated design approach is based on the proportional navigation concept, in the sense that the flight control system is designed with the objective of driving the line-of-sight rates to zero. The integrated guidance-autopilot system is also responsible for stabilizing the kinetic warhead dynamics.

In order to design the integrated flight control system using the Nonlinear Synthesis Tools[17] software package, it is necessary to provide information on the order of

differentiation which would otherwise have to be carried out analytically by the designer. The control influence chains were defined as:

$$u_z \rightarrow \dot{\delta}_z \rightarrow \delta_z \rightarrow q \rightarrow w \rightarrow \dot{\lambda}_z \tag{18}$$

$$u_y \rightarrow \dot{\delta}_y \rightarrow \delta_y \rightarrow r \rightarrow v \rightarrow \dot{\lambda}_y \tag{19}$$

These relationships describe the interdependence of control and state variables in the kinetic warhead dynamics. For instance, (18) suggests that the force u_z acting on the moving mass influences the velocity $\dot{\delta}_z$ and position δ_z of the moving mass along the z-axis, which in turn influences the kinetic warhead pitch rate q resulting in a change in the body velocity component w along the z-axis. In the presence of external forces this velocity component will result in an acceleration component normal to the kinetic warhead, which will then influence the line-of-sight rate $\dot{\lambda}_z$. Expression (18) denotes the same process in the yaw axis. The software package uses these relationships to construct the feedback linearizing map and to design the pseudo-control laws. Appendix A provides some more details on the feedback linearization process.

3.1.1 Engagement Scenario 1

The first engagement scenario used to evaluate the integrated guidance-autopilot system is described below. The closed-loop poles in both channels were {-51, -50, -35, -30, -20}. The kinetic warhead and target trajectories are shown in Figure 4 and Figure 5.

This engagement scenario is similar to the endo-atmospheric engagement considered in Reference 3 in which both the warhead and target are initially at an altitude of 45,000 ft, and 50,000 ft. apart. Both vehicles have 15-degree flight path angles and are on reciprocal headings, and both have an initial velocity of 6000 ft/sec. In addition, the target has an initial offset of 1000 ft. in the east direction.

The line of sight rates are shown in Figure 6. The integrated guidance-autopilot drives the line-of-sight rates to near-zero early in the engagement, and then attempts to keep it there. Note that it is possible to introduce dynamic compensation networks in the integrated guidance-autopilot to distribute the control effort more uniformly over the engagement. Moreover, the gain in the line-of-sight rate states can be increased to further reduce the miss distance. The miss distance for this engagement was 0.28 ft.

The angle of attack and angle of sideslip are shown in Figure 7. There is a large initial acceleration seen in Figure 8, particularly in the lateral channel, to remove the LOS error. A noticeable roll rate is induced due to the moving masses, which can be seen in the angular velocities shown in Figure 9. The actuator mass displacements are shown in Figure 10.

3.1.2 Engagement Scenario 2

The second scenario is the exo-atmospheric case from Reference 5 where the warhead and target start at an altitude of 545,000 ft. and are 120,000 ft. apart on reciprocal headings and flight path angles of 45 degrees. Both vehicles have an initial velocity of 6000 ft/sec. In this case the poles had to be slowed down due to the smaller force available for steering. The closed loop poles were chosen to be {-51, -50, -25, -20, -10} in both channels. The kinetic warhead and target trajectories are shown in Figure 11.

The line of sight rates are shown in Figure 12. The miss distance was 0.42 ft. As in the previous engagement scenario, the integrated guidance-autopilot system proceeds to correct most of the line-of-sight rates at the beginning of the engagement. The angle of attack and angle of sideslip histories are shown in Figure 13. The acceleration components are seen in Figure 14. In this case the acceleration components perpendicular to the velocity vector are shown instead of the body frame as was shown in the atmospheric case. This is due the fact that the maneuvering forces are derived from pointing the thrust vector, which acts along the kinetic warhead's longitudinal axis. Acceleration components normal to the velocity vector can thus be controlled, whereas the lateral and normal acceleration components along the body axes cannot.

As in the atmospheric interception scenario, there is a large increase in acceleration at the beginning of the engagement. Note that since the thrust is 500 lbf and the total mass is 70 lbm, the maximum acceleration obtainable is around 7 g's. Figure 13 shows that the maximum angle of attack during the engagement was about 68 degrees. The flight control system delivers good performance even in the presence of large angles of attack. Note that this fact has important bearing on the types of seekers that can be employed in conjunction with the moving mass control of kinetic warheads.

Engagements can be accomplished with smaller angle of attack and angle of sideslip if higher thrust levels are available. The angular velocities are shown in Figure 15. The actuator mass displacements are shown in Figure 16.

3.1.3 Engagement Scenario 3

This engagement features a weaving target example from Reference 5. The warhead and target are initially at an altitude of 45,000 ft. and are headed directly toward each other. The initial velocities are 6000 ft/sec. for both vehicles. The target weaves in the vertical plane with an acceleration of 3 g and a frequency of 0.5 Hz. The poles of the integrated flight control system were chosen to be the same as in Subsection 3.1.1.

The kinetic warhead and target trajectories are shown in Figure 17. The line of sight rates are shown in Figure 18. As in the previous engagement scenarios, the flight control system attempts to maintain the line-of-sight rates close to zero. However, it encounters difficulties due to the target maneuvers. The angle of attack and angle of sideslip histories are shown in Figure 19. The actuator mass displacements are shown in Figure 20. The terminal miss distance for this case was 0.28 ft.

4. Conclusions

This paper described the modeling, simulation, and integrated guidance and control of a kinetic warhead utilizing moving-mass actuators. The moving-mass actuation methodology can be used in any speed range both in the atmosphere as well as outside it, as long as there is a force, either aerodynamic or propulsive, acting on the vehicle. Since the actuators are contained entirely within the airframe geometric envelope, and because there are no jet interaction effects to alter the vehicle's aerodynamics or to obscure electro-optical sensors, the moving-mass actuation technique offers several advantages over conventional aerodynamic control surfaces and reaction control systems. The disadvantages of the moving-mass actuation technology are that the airframe must provide adequate internal space for the moving masses, and must have near-neutral aerodynamic static stability characteristics. The present work has developed a 9 degree-of-freedom simulation model of a kinetic warhead with three moving-mass actuators.

This simulation model was used for actuator sizing and in the development of flight control systems.

A software package for performing a numerical feedback linearization technique, developed under a previous research effort, was used to design nonlinear flight control systems. Pole placement was used to design the control law for the feedback linearized system. An integrated design methodology was described, based on regulating the line-of-sight rates between the vehicle and the target. Interception of non-maneuvering and weaving targets was demonstrated, as was interception in both endo-atmospheric and exo-atmospheric conditions. In every case, the moving mass integrated guidance-autopilot was able to deliver a miss distance smaller than half the diameter of the kinetic warhead. Improvements in the accuracy of the guidance-autopilot system design should be feasible through the introduction of dynamic compensators in the flight control loop.

Future research will examine the impact of disturbances, sensor errors, and uncertainties in the target maneuvers on the kinetic warhead performance, and will investigate approaches for making the system robust to these uncertainties. Application of the moving-mass control technology to other flight vehicles and underwater vehicles will also be of future interest.

Appendix A: Numerical Feedback Linearization

The feedback linearization of the KW dynamics is achieved by redefining the system dynamics in terms of the line of sight rates. It may be observed from Section 2 that the forces on the moving masses, the control variables in the present problem, will appear in the fifth derivative of the line of sight rates. Hence, feedback linearization can be achieved by redefining the KW dynamics in terms of the line of sight rates and four of its successive derivatives as the state variables.

Starting from expressions (18) and (19) the software package[17] numerically carries out this operation. It can be seen from Equation (15) that the line-of-sight rates are functions of position and velocity, say

$$\dot{\lambda} = f_1(\vec{r}, V_O) \qquad \text{(A.1)}$$

Differentiating this expression five times will produce a complex expression of the form:

$$\lambda^{VI} = \phi(\cdot) + \psi(\cdot)u \tag{A.2}$$

where $\phi(\cdot)$ and $\psi(\cdot)$ are complex nonlinear functions that depend on the states of the KW and moving masses. Defining the state variables as $z = \left[\lambda\ \dot{\lambda}\ \ddot{\lambda}\ \dddot{\lambda}\ \lambda^{IV}\ \lambda^{V}\right]^T$, the KW dynamics can be recast in the form:

$$\dot{z} = Az + Bv \tag{A.3}$$

where

$$A = \begin{bmatrix} 0 & 1 & 0 & 0 & 0 \\ 0 & 0 & 1 & 0 & 0 \\ 0 & 0 & 0 & 1 & 0 \\ 0 & 0 & 0 & 0 & 1 \\ 0 & 0 & 0 & 0 & 0 \end{bmatrix}, B = \begin{bmatrix} 0 \\ 0 \\ 0 \\ 0 \\ 1 \end{bmatrix} \tag{A.4}$$

and the pseudo-control variable v is given by:

$$v = \phi(\cdot) + \psi(\cdot)u \tag{A.5}$$

The nonlinear control system design software automatically constructs the nonlinear functions $\phi(\cdot)$ and $\psi(\cdot)$ from the simulation model of the KW. Since the transformed system is in a linear, time-invariant form with respect to the pseudo-control variable, linear control techniques can be used to design a stable feedback control law; i.e.:

$$v = [k_1\ \ k_2\ \ k_3\ \ k_4\ \ k_5]\, z \tag{A.6}$$

In the present study, pole placement was used to compute the gains using standard techniques. The actual control variables can be recovered from the pseudo control variables using the inverse relationship from (A.5):

$$u = \psi^{-1}(\cdot)[v - \phi(\cdot)]$$

If the system nonlinearities $\phi(\cdot)$ and $\psi(\cdot)$ are known reasonably well, the resulting closed-loop system will have dynamic properties close to the transformed system.

Acknowledgement

This research was supported by the U. S. Navy, Contract No. N00178-01-C-1020. The authors would like to thank Dr. Pashang Esfandiari and Mr. Mick Blackledge of the Missile Defense Agency for their interest in and support of this work.

References

[1]Chanute, O., *Progress in Flying Machines*, Dover, Mineola, NY, 1997. p. 93.

[2]Wolko, H. S. (Editor), *The Wright Flyer*, Smithsonian Institution Press, Washington, D. C., 1987, p. 48.

[3]Robinett, R. D., Sturgis, B. R., and Kerr, S. A., "Moving Mass Trim Control for Aerospace Vehicles," *Journal of Guidance, Control, and Dynamics*, V. 19, No. 5, 1996, pp. 1064-1070.

[4]Petsopoulos, T., and Regan, F.J., "A Moving-Mass Roll Control System for a Fixed-Trim Reentry Vehicle," AIAA Paper 94-0033, January, 1994.

[5]Chadwick, W. R., and Malyevac, D. S., "Considerations on the Design of Kinetic Kill Interceptor with Moving Mass Control", Report # NSWCDD TR-00/87, Naval Surface Warfare Center, Dahlgren, VA, August, 2000.

[6]Menon, P. K., Iragavarapu, V. R., and Ohlmeyer, E. J., "Integrated Design of Agile Missile Guidance and Control System", *AIAA Missile Sciences Conference*, AIAA, Reston, VA, 1998.

[7]Menon, P. K., and Ohlmeyer, E. J., "Integrated Guidance-Control Systems for Fixed-Aim Warhead Missiles", *AIAA Missile Sciences Conference*, AIAA, Reston, VA, 2000.

[8]Cloutier, J. R., D'Souza, C. N., and Mracek, C. P., "Nonlinear Regulation and Nonlinear H_∞ Control Via the State-Dependent Riccati Equation Technique", *Proceedings of the International Conference on Nonlinear Problems in Aviation and Aerospace*, AIAA, Reston, VA, 1996.

[9]Mracek, C.P. and Cloutier, J. R., "Full Envelope Missile Longitudinal Autopilot Design using the State-Dependent Riccati Equation Method", *Proceedings of the AIAA Guidance, Navigation and Control Conference*, AIAA, Reston, VA, pp. 1697-1705.

[10]Cloutier, J. R., "State-Dependent Riccati Equation Techniques: An Overview", *Proceedings of the American Control Conference*, Institute of Electrical and Electronics Engineers, Piscataway, NJ, pp. 932-936.

[11] Isidori, A., *Nonlinear Control Systems - An Introduction*, Springer-Verlag, New York, 1989, pp. 145-172.

[12] Marino, R., and Tomei, P., *Nonlinear Control Design*, Prentice Hall, New York, NY, 1995, pp. 41-60.

[13] Menon, P. K., Badgett, M. E., Walker, R. A., and Duke, E. L., "Nonlinear Flight Test Trajectory Controllers for Aircraft", *Journal of Guidance, Control, and Dynamics*, Vol. 10, No. 1, 1987, pp. 67-72.

[14] Lane, S. H., and Stengel, R. F., "Flight Control Design Using Nonlinear Inverse Dynamics", *Automatica*, Vol. 24, No. 4, 1988, pp. 471-483.

[15] Meyer, G., and Cicolani, L., "Application of Nonlinear Systems Inverses to Automatic Flight Control Design System Concepts and Flight Evaluation," *Theory and Applications of Optimal Control in Aerospace Systems*, AGARDograph 251, P. Kant (Editor), July, 1981.

[16] Menon, P. K. and Ohlmeyer, E. J., "Integrated Design of Agile Missile Guidance and Autopilot Systems", *IFAC Journal of Control Engineering Practice*, Vol. 9, 2001, pp. 1095-1106.

[17] Menon, P. K., et al., *Nonlinear Synthesis Tools™ for Use with MATLAB®*, Optimal Synthesis Inc., Palo Alto, CA, 2000.

[18] Menon, P. K., Iragavarapu, V. R., and Ohlmeyer, E. J., "Nonlinear Missile Autopilot Design Using Time-Scale Separation," *Proceedings of the 1997 AIAA Guidance, Navigation, and Control Conference*, AIAA, Reston, VA, 1997, pp. 1791-1803.

[19] Menon, P. K., Iragavarapu, V. R., and Ohlmeyer, E. J., "Software Tools for Nonlinear Missile Autopilot Design," AIAA Paper 99-3975.

[20] Anon., *Using Simulink®*, The MathWorks, Inc., Natick, MA, 2000.

[21] Kane, T. R. and Levinson, D. A., *Dynamics: Theory and Applications*, McGraw-Hill, New York, NY, 1985.

[22] Palumbo, N. F., and Jackson, T. D., "Integrated Missile Guidance and Control: A State Dependent Riccati Differential Equation Approach", *1999 IEEE International Conference on Control Applications*, Institute of Electrical and Electronics Engineers, Piscataway, NJ, pp. 243-248.

[23] Menon, P. K., Dewell, L. D., and Sweriduk, G. D., "Integrated Guidance-Autopilot Designs for Anti-Jam Operation of Precision Munitions", Final Report prepared under Air Force Contract No. F08630-99-C-0040, Optimal Synthesis Inc., Palo Alto, CA, January 2000.

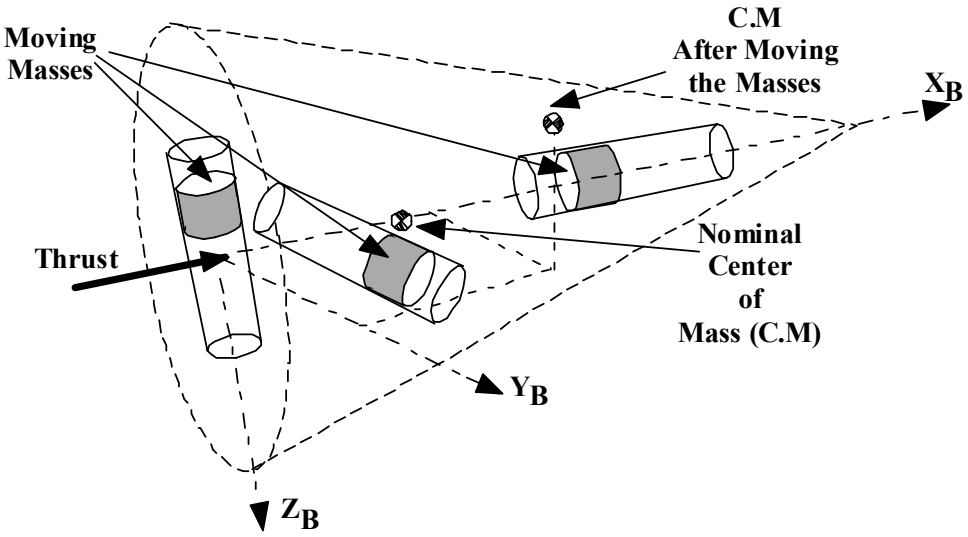

Figure 1. Moving-mass Kinetic Warhead Concept

JOURNAL OF GUIDANCE, CONTROL, AND DYNAMICS
Vol. 27, No. 1, January-February 2004, pp. 118 - 126.

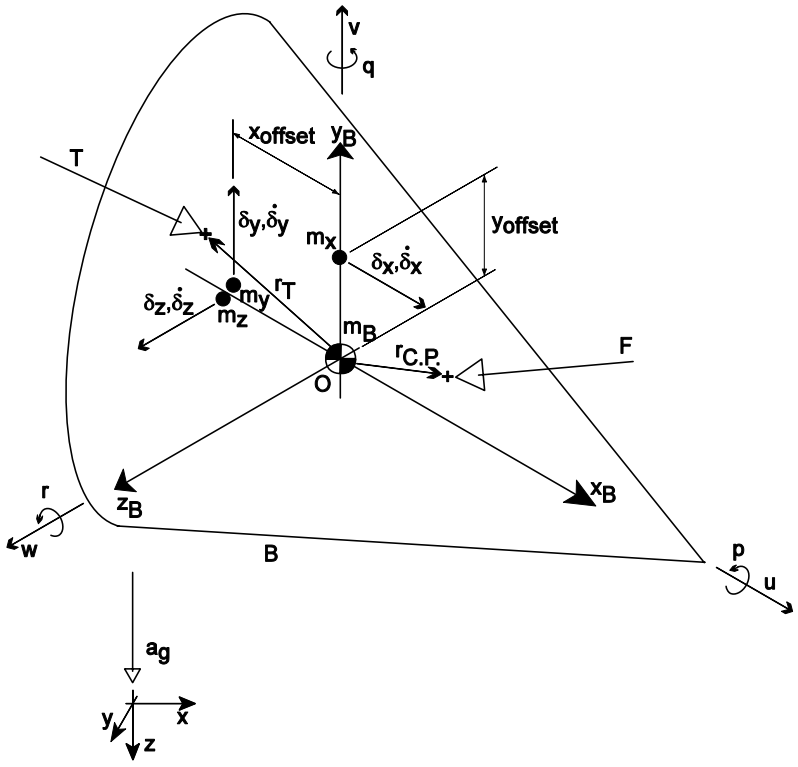

Figure 2. Kinetic Warhead

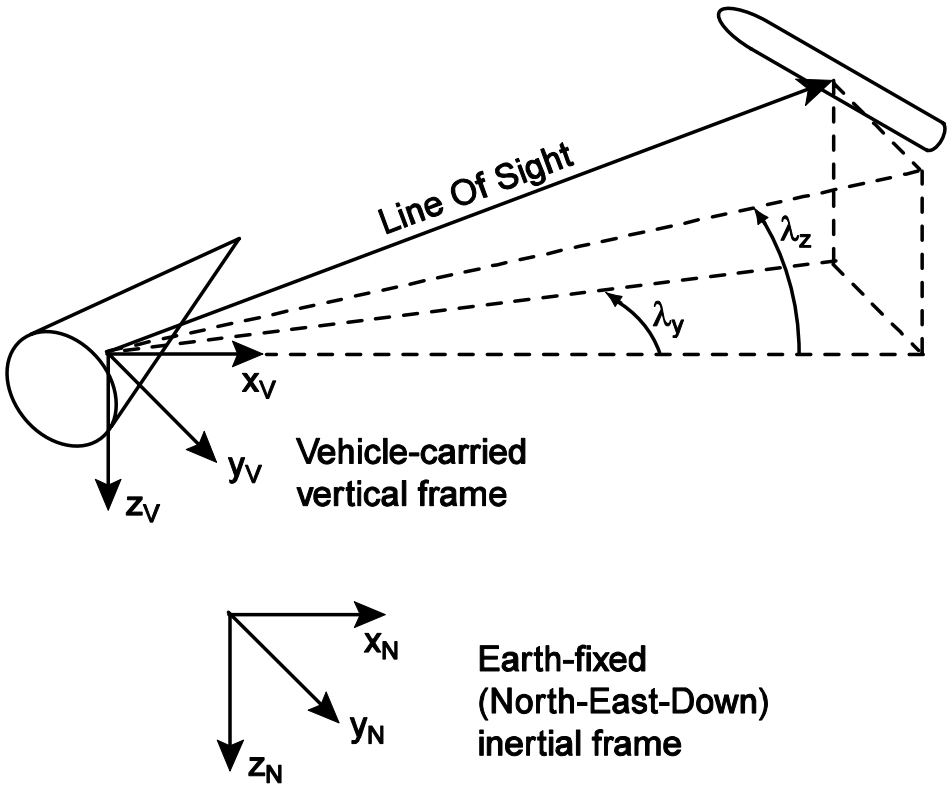

Figure 3. Line Of Sight Angles

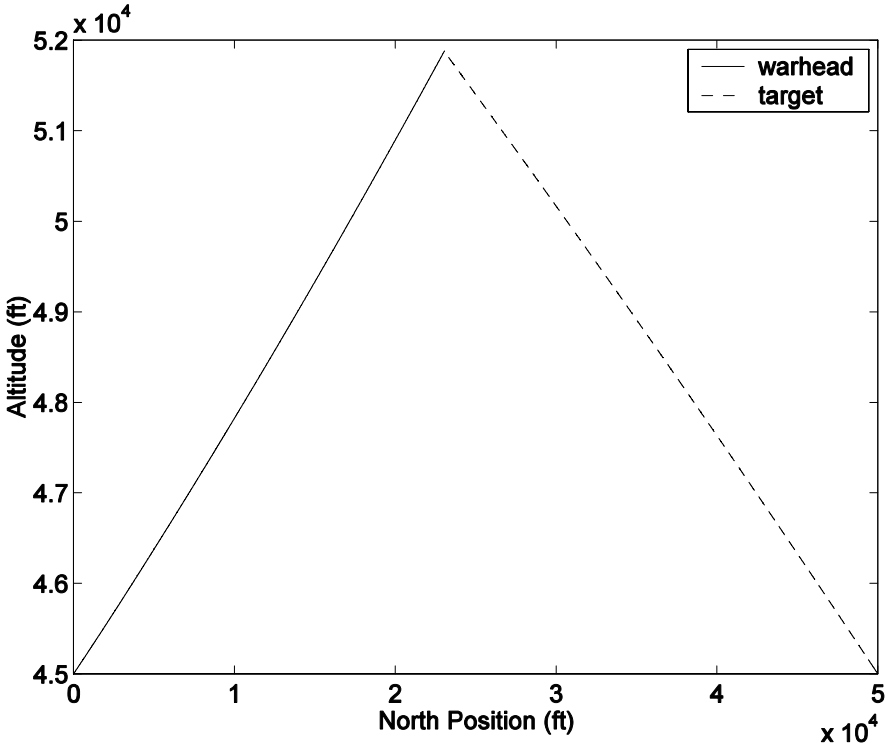

Figure 4. Warhead and Target Trajectories, Vertical Plane

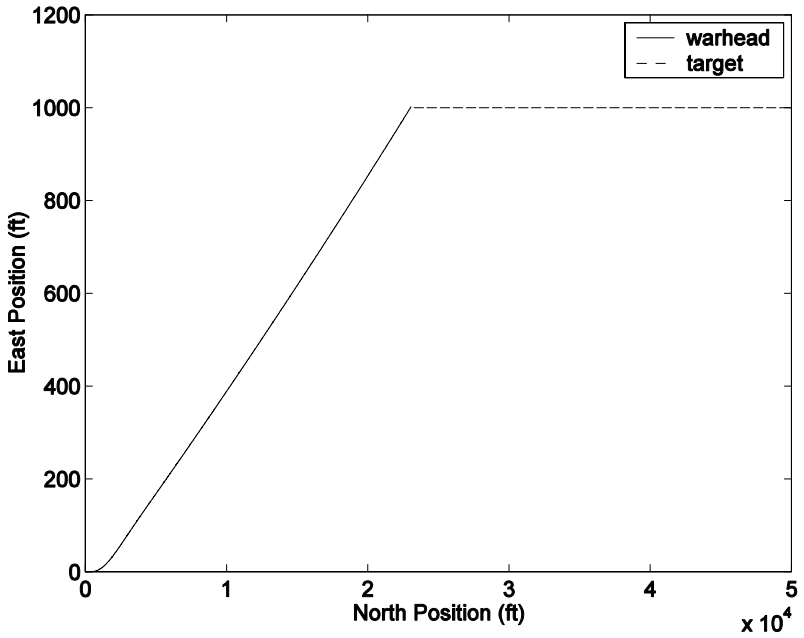

Figure 5. Warhead and Target Trajectories, Horizontal Plane

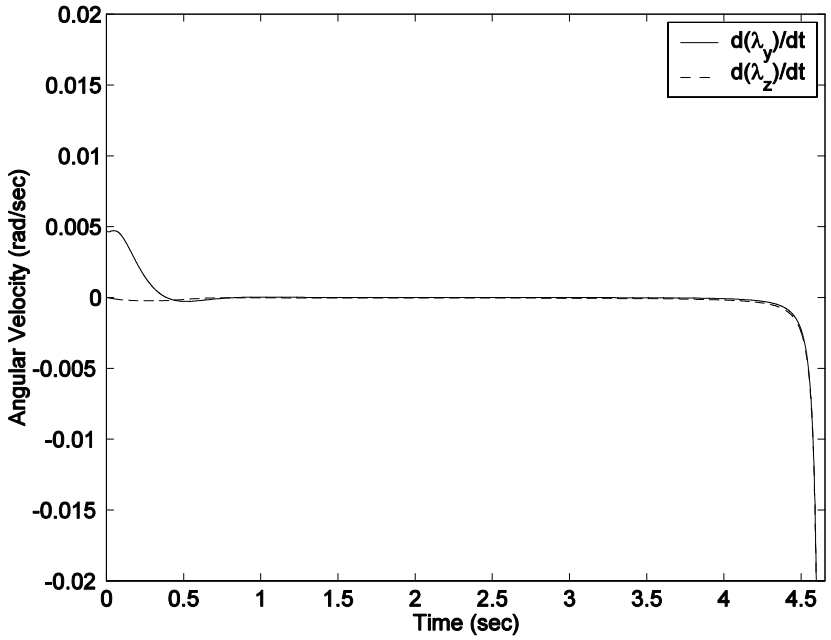

Figure 6. Line Of Sight Rates vs. Time

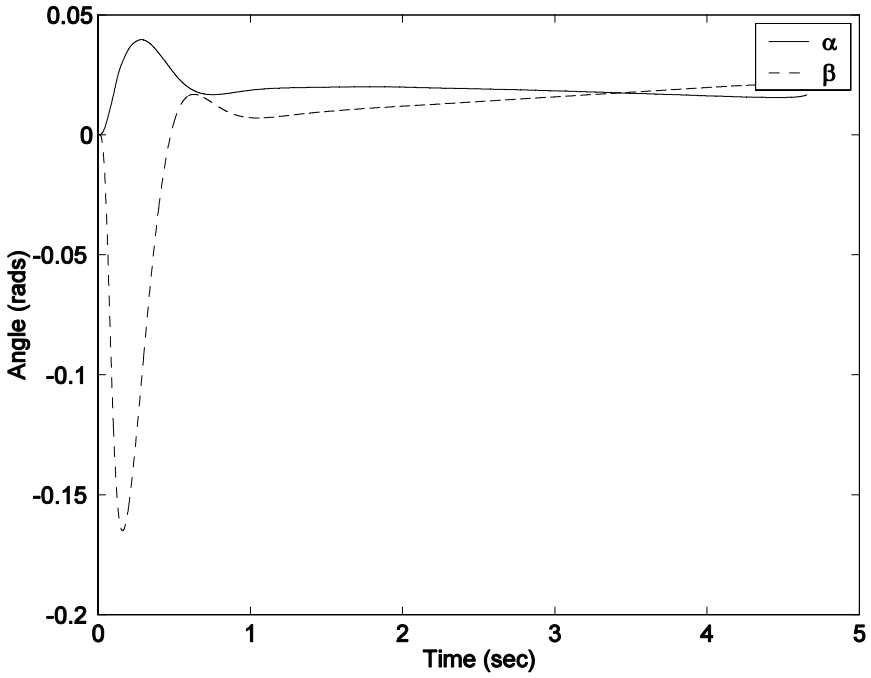

Figure 7. Angles of Attack and Sideslip vs. Time

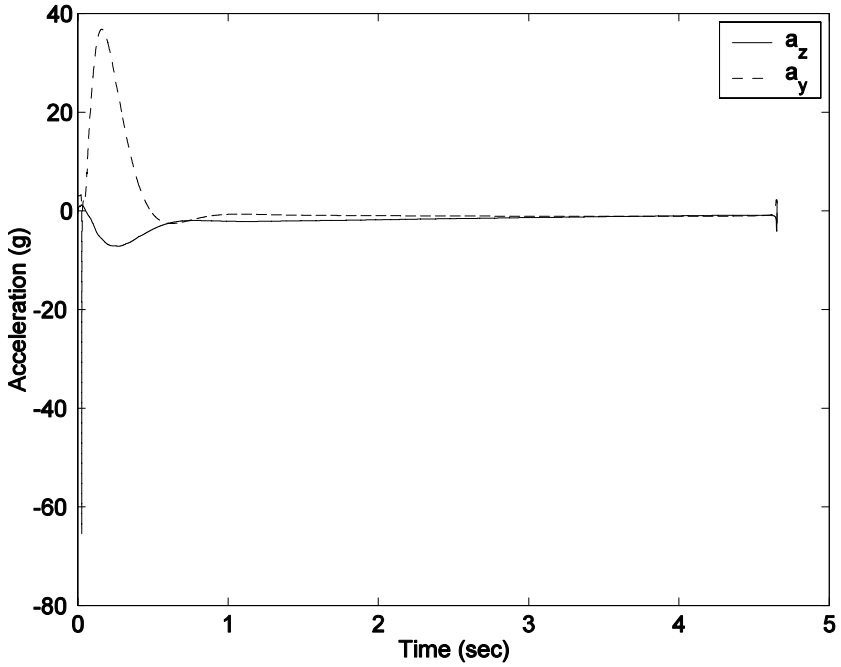

Figure 8. Body-Frame Accelerations vs. Time

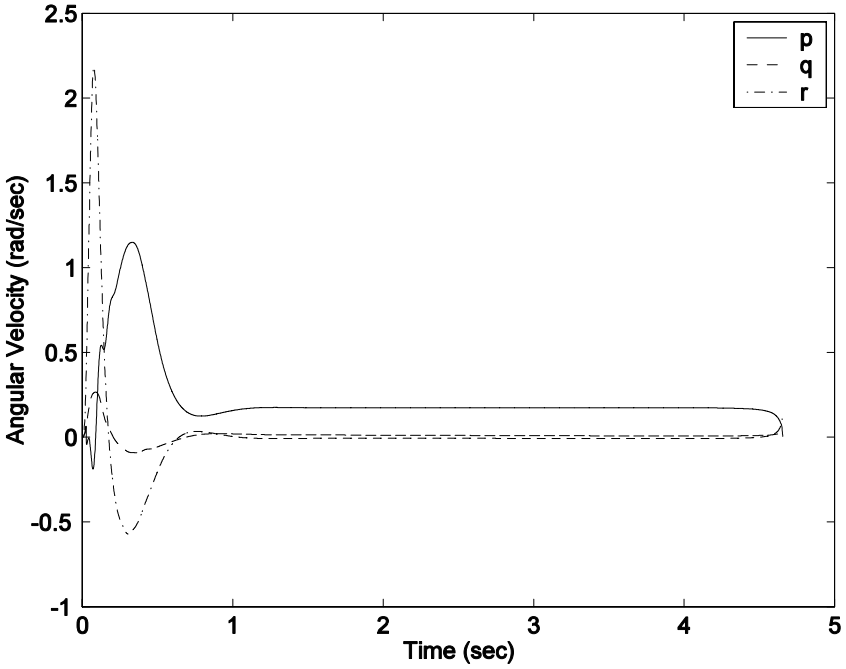

Figure 9. Body Angular Velocities vs. Time

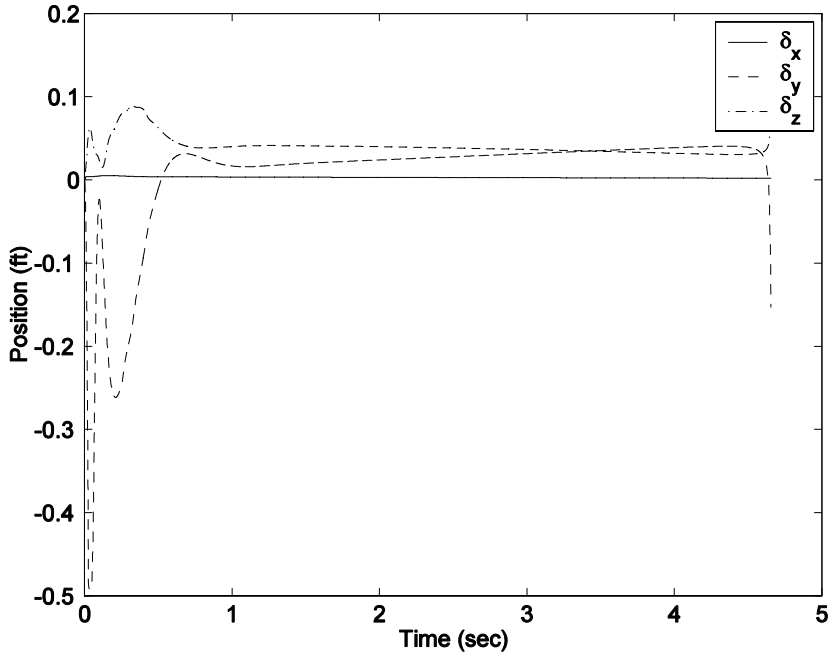

Figure 10. Actuator Mass Displacements vs. Time

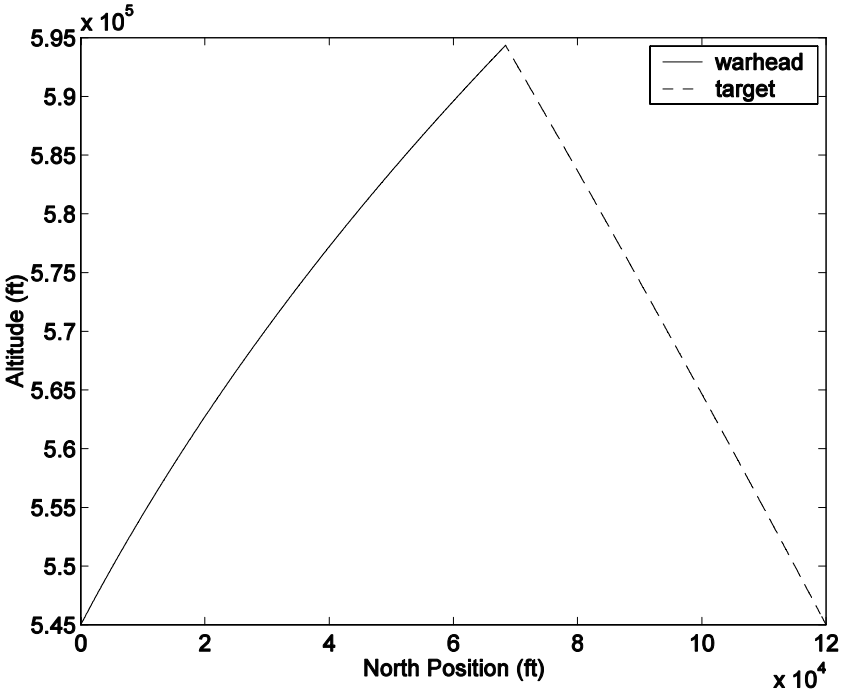

Figure 11. Warhead and Target Trajectories, Vertical Plane

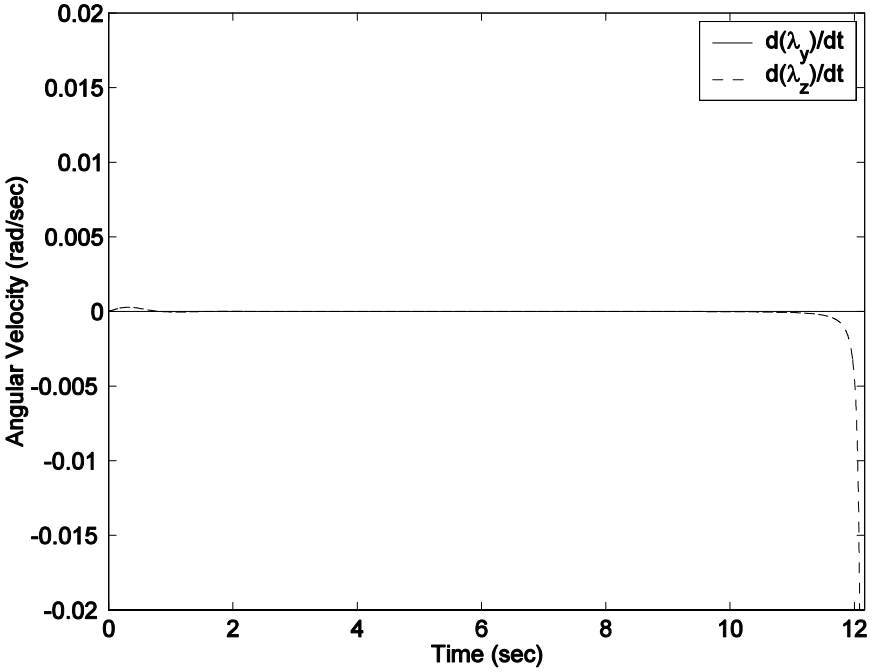

Figure 12. Line of Sight Rates vs. Time

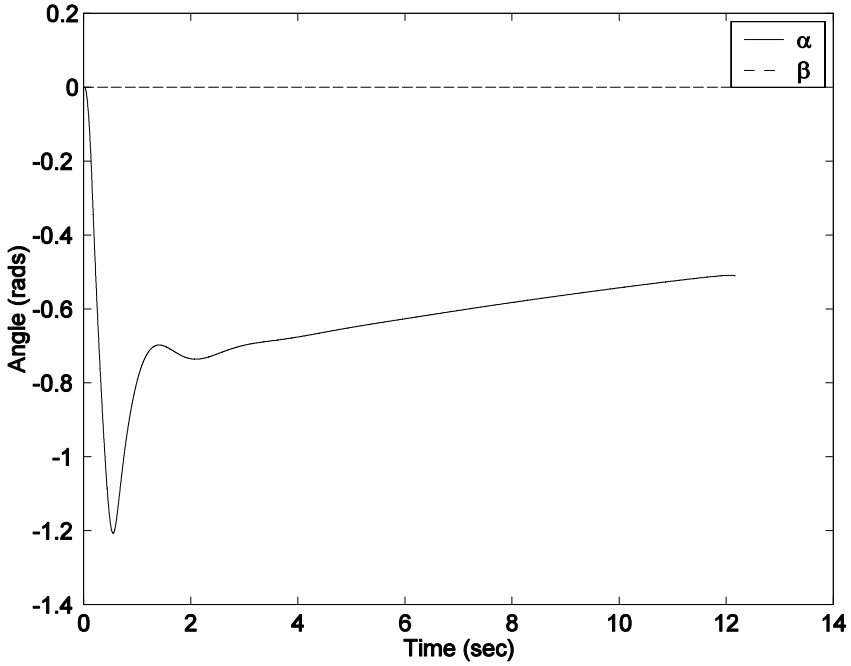

Figure 13. Angles of Attack and Sideslip vs. Time

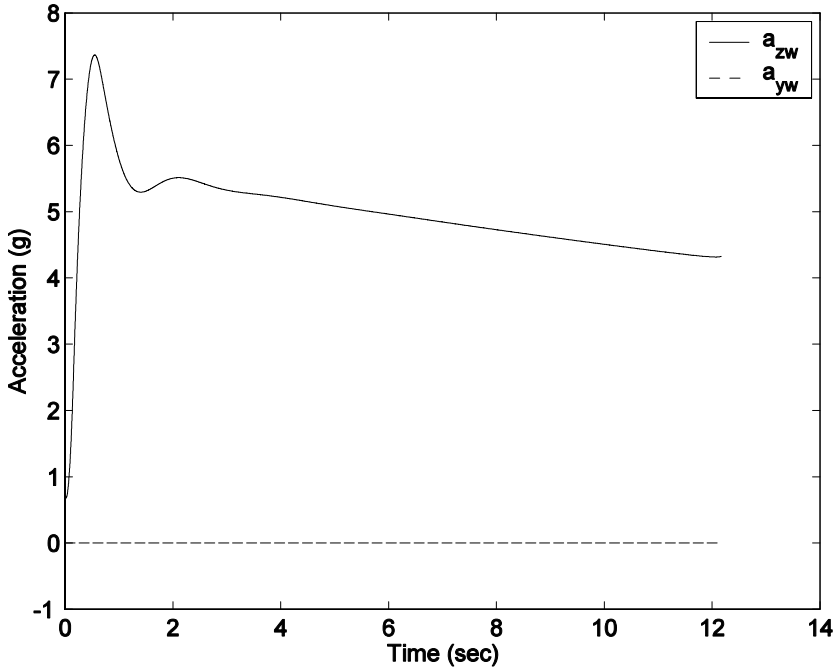

Figure 14. Accelerations vs. Time

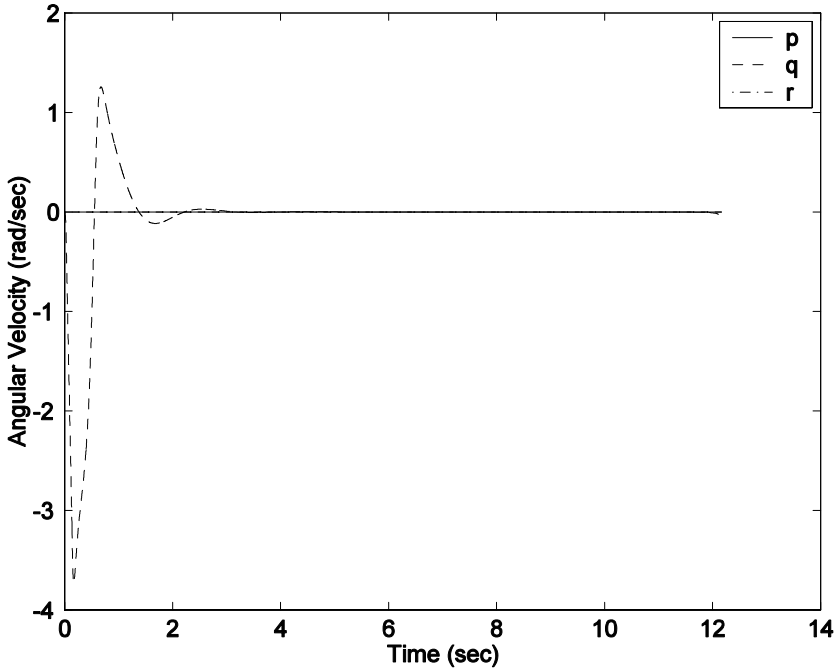

Figure 15. Body Angular Velocities vs. Time

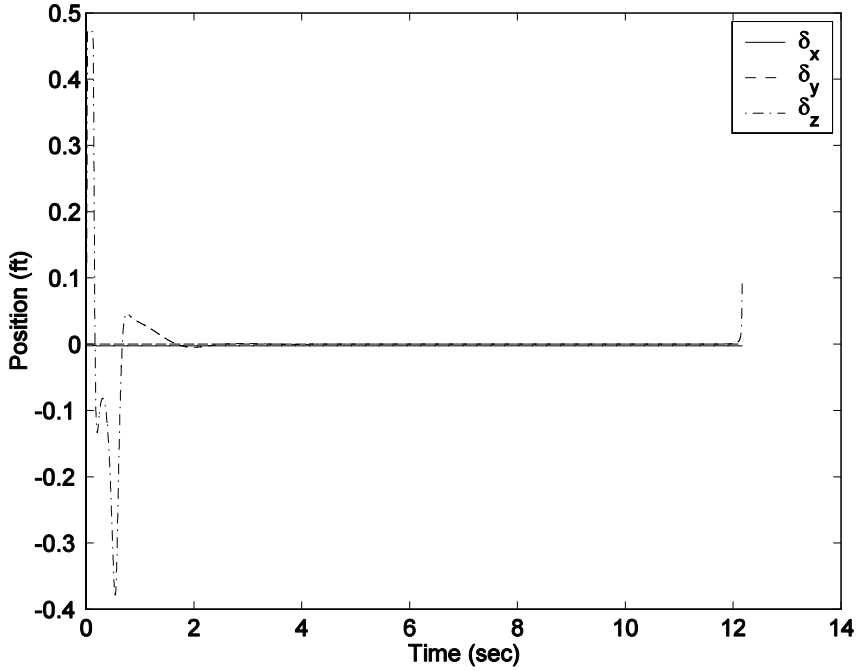

Figure 16. Actuator Mass Displacements vs. Time

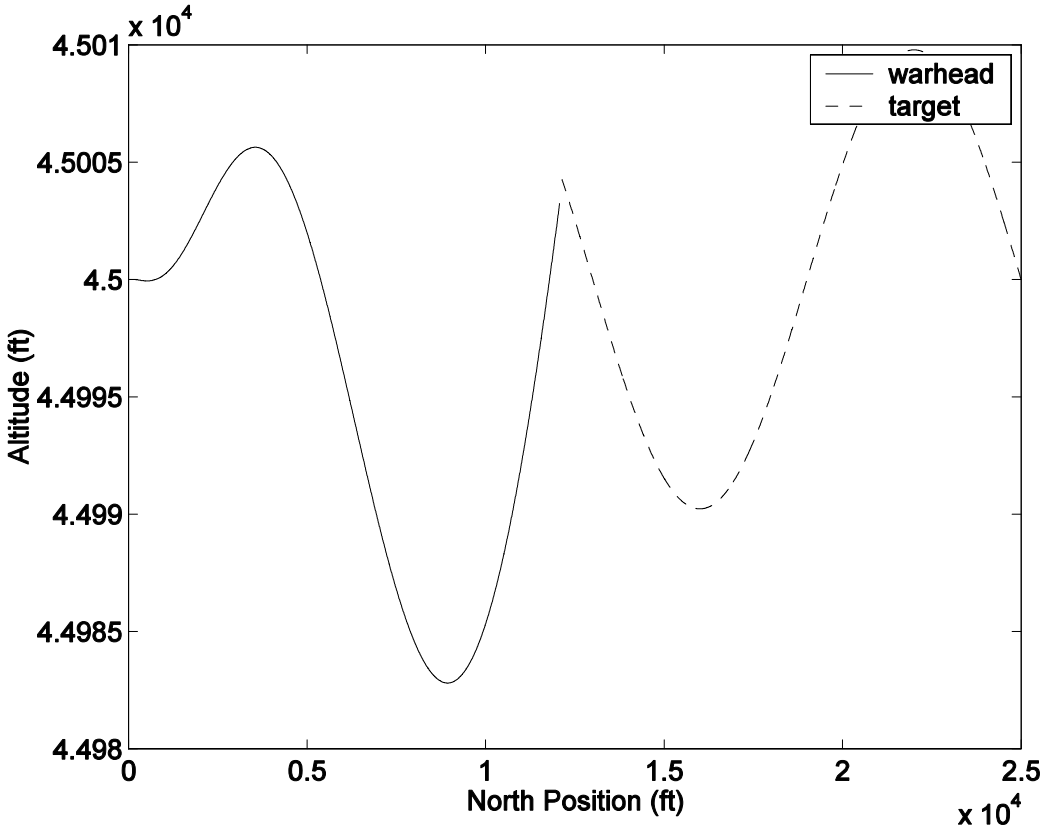

Figure 17. Warhead and Target Trajectories, Vertical Plane

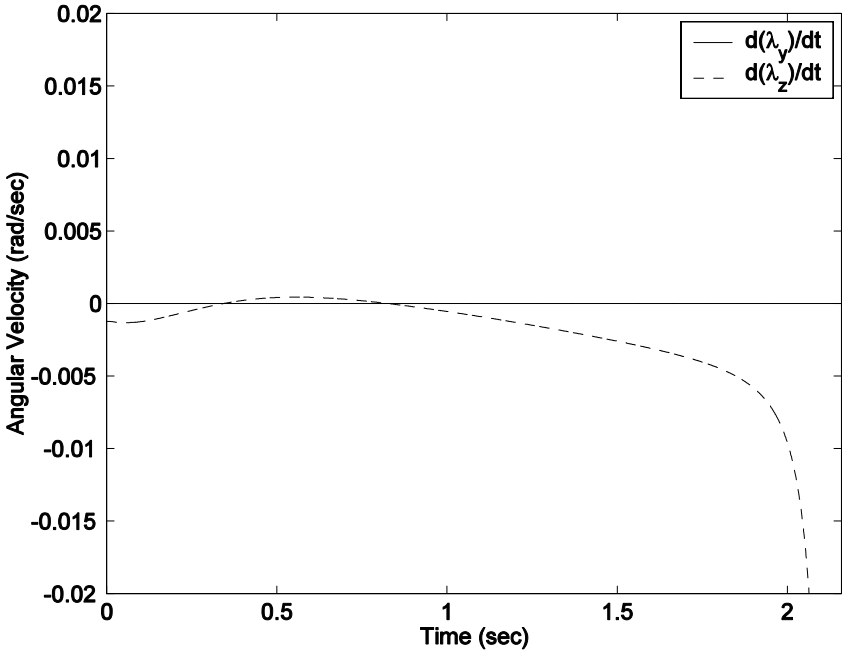

Figure 18. Line of Sight Rates vs. Time

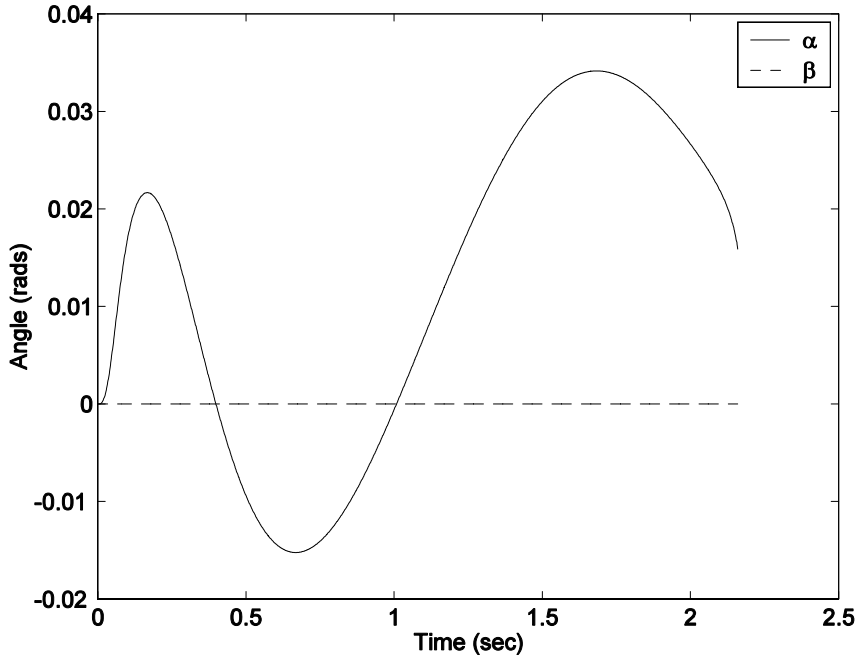

Figure 19. Angles of Attack and Sideslip vs. Time

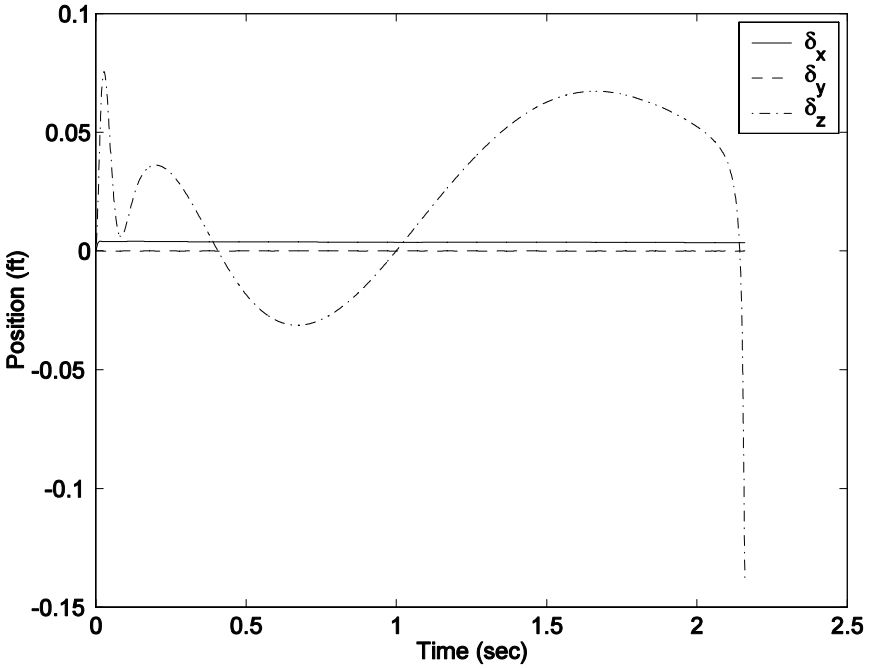

Figure 20. Actuator Mass Displacements vs. Time